Potential energy and free energy surfaces of glycyl-phenyalanyl-alanine (GFA) tripeptide: experiment and theory

Haydee Valdes,[a] Vojtech Spiwok,[b] Jan Rezac,[a] David Reha,[c] Ali G. Abo-Riziq[d], Mattanjah S. de Vries, [d] Pavel Hobza[a,*]

a) Institute of Organic Chemistry and Biochemistry, Academy of Sciences of the Czech Republic and Center for Biomolecules and Complex Molecular Systems, 166 10 Prague 6, Czech Republic. FAX: +420-220 410 320

b) Department of Biochemistry and Microbiology. Institute of Chemical Technology of Prague. Technicka 3, 166 28 Prague 6, Czech Republic.

c) IRC Polymer and Complex Fluids. School of Physics and Astronomy. University of Leeds. Leeds. LS2 9JT. UK

d) Department of Chemistry and Biochemistry, University of California Santa Barbara, CA 93106, USA

e-mail: pavel.hobza@uochb.cas.cz

Abstract

The free energy surface (FES) of glycyl-phenyalanyl-alanine (GFA) tripeptide was explored with molecular dynamic simulations in combination with high level correlated ab initio quantum chemical calculations. The molecular dynamics employed the tight-binding DFT method, accounting for the dispersion energy, instead of the AMBER empirical force field, which yielded inaccurate results. We classified the minima, localized in the FESs, according to two different criteria namely: (a) the

backbone conformational arrangement and its resemblance to the secondary structure of proteins (families β_L, 3_{11}, γ and γ -3_{11}); and (b) the existence of a COOH···O=C intramolecular H-bond between the hydrogen of the terminus carboxyl group and the backbone CO of residue *i+1* (families CO_2H_{free} and CO_2H_{bonded}). Comparison with experiment shows that the theoretically predicted most stable minima in the FES correspond to the observed experimentally structures and the theoretically scaled frequencies match reasonably well those measured spectroscopically. Remarkably, however, we do not experimentally observe the CO_2H_{bonded} family, although its stability is comparable to that of the CO_2H_{free} structures. Motivated by this result we reinvestigated the FES of GFA with a completely different method, metadynamics, which includes the anharmonic effects. This is the first combination of the metadynamics approach with the tight-binding DFT-D procedure. Metadynamics confirms the existence and comparable stability of the two families of structures. The fact that we do not observe structures of the CO_2H_{bonded} experimentally was explained by their short excited state lifetime. Additionally, we also carried out ab initio calculations using DFT theory either in its augmented version by dispersion interaction (DFT-D) or by using the M06-2X functional. The importance of the dispersion energy in stabilizing peptide conformers is well reflected by our pioneer analysis using the DF-DFT-SAPT method on the nature of the backbone/side chain interactions.

Introduction

The secondary structure of proteins is defined to a large extent by a network of hydrogen bonds between the backbone amide groups (-C(O)-N-H···O=C)[1] but other non-covalent interactions play a structural role as well. Steiner and Koellner[2] have stressed the importance of the X-H···π H-bonds (X= N, O, S) in the stabilization of termini of helices, ends and edges of strands, B-bulges and turns. These structural motifs include H-bonds from peptide N-H groups, i.e. N-H···π H-bonds, which are known to be formed quite frequently. [2-6] Amide-aromatic interactions have been the subject of a number of theoretical and experimental studies, both in aqueous solution[7,8] and in the gas phase.[9] N-H···π H-bonds in proteins have typically been modeled by much simpler systems such as isolated ammonia-benzene,[10,11] formamide-benzene,[12-14] N-methylformamide-benzene[12,15] and N-methylacetamide[12] molecular complexes. In essence, these studies focused on the calculation of the stabilization energies of these complexes by means of density functional theory (DFT) and/or wave-function theory (WFT) methods. These calculations provided an estimation of the strength of the hypothetically analog interaction in proteins. In the model systems the orientation of the amide moiety relative to the benzene ring depends primarily on the electrostatic force and is also affected by dispersion and electrostatic interactions (e.g. dipole(NH)-quadrupole(benzene)).

While very valuable, these prototype systems do not model the N-H···π interactions occurring in proteins completely accurately. Geometries in the simpler models are quite unrealistic because the interacting monomers adopt an optimal geometry minimizing the energy of the given complex with no hint of any of the geometrical restrictions present in proteins. First it is well known that the orientation of the peptide bonds (modeled by the free ammonia, formamide, N-methylformamide or N-methylacetamide) depends on the values of the φ and ψ backbone dihedral angles, as defined in Ramachandran plots. Secondly, the nitrogen of the amide groups tends to adopt the orientation in which it achieves its maximal hydrogen-binding capacity, forming additional H-bonds.[8,16-18] This geometrical arrangement can work *against* the nitrogen´s optimal interaction with the aromatic side chain, as modeled by a free benzene in the prototype systems but known to be mainly constrained to the gauche+ (g^+), gauche-

(g^-) or trans(a) orientations in proteins. In peptides or proteins the nature of the backbone-aromatic side chain interaction is quite delicate. Studies performed on model systems so far suggest that a subtle modification in the geometry of the system can result in a significantly different forces scenario. Therefore we wish to investigate to what extent conclusions drawn from the model systems can be extrapolated to real geometries of isolated peptides.

To this end we have studied the glycyl-phenyalanyl-alanine (GFA) tripeptide. In order to work with real gas-phase structures we have proceeded as follows. First, we have scanned the potential energy surface (PES) by means of the tight-binding DFT method covering the London dispersion energy (DF-TB-D) (see more detailed information in the computational details and methods section) finding all the existing minima in the PES. This is a critical step and the use of a DFT-D based procedure in the first screening of the PES is essential. When instead of an 'accurate' DFT method an empirical force field is applied, inaccurate structures result. This is mainly due to the fact that the DFT-D procedure is free of problems with the definition of atomic charges and properly covers the dispersion energy. Second, we recalculated the most stable conformers using both, DFT and WFT methods. In the next step the thermodynamic characteristics were determined on the basis of standard statistical thermodynamic calculations based on the rigid rotor-harmonic oscillator-ideal gas (RR-HO-IG) approximation. This is another critical step and here again a proper evaluation of the free energy surface (FES) is essential. The harmonic approach and/or empirically based calculations are questionable to some extent. The thermodynamic characteristics are mainly determined from low-frequency modes and anharmonic effects are for these modes critical. For this reason, we have also scanned the FES using metadynamics,[19,20] a free energy modeling technique effectively covering anharmonic effects, which is used here for the first time in combination with tight-binding DFT-D. The approximate DFT-D method is thus used systematically in evaluating the PES and FES. Next, we made a prediction which structures should be observed experimentally, which we verified by comparing the theoretical frequencies with experimental gas phase infrared (IR) spectra. Finally, we studied the conformational preferences of the peptide backbone and the nature of the backbone-aromatic side chain interaction in the GFA tripeptide. This constitutes, to our

knowledge, the first study of the nature of backbone-aromatic side chain interactions performed on the basis of real gas-phase peptide structures and an ab initio quantum chemical methodology.

At the same time, we take advantage of this system to continue with the assessment of the performance of the DFT-D method (Density Functional Theory augmented with an empirical dispersion term)[21] in the study of isolated small peptides which we began in earlier work for the tryptophyl-glycine (Trp-Gly) and tryptophyl-glycyl-glycine (Trp-Gly-Gly) peptides.[22] We have extended our former database of 30 different peptide conformers by another 16 structures for which we have compared the DFT-D electronic relative energies and geometries with CCSD(T)/CBS energies and RI-MP2/cc-pVTZ geometries, respectively. These results will be further included in an extensive benchmark database of accurate relative energies and geometries of isolated small peptides that we are currently preparing. Furthermore, we verified our prediction of the most stable conformers on the DFT-D FES against the experimental results. Additionally, we have assessed the newly developed M06-2X functional particularly developed to cover the London dispersion energy.[23] Assessing the DFT-D -or any other- methodology or new functional is of particular relevance in the quantum chemical calculation of the structure and properties of isolated peptides, particularly those containing at least one aromatic side chain. A vast majority of the functionals used for the DFT calculations fails for the study of systems where the dispersion energy is an important component of the stabilization energy[24-26] and the MP2 method (even with the resolution of identity approximation) is already at the edge of its computational-time applicability for a tripeptide. Thus, even when accurate, the study by means of WFT methods becomes very tedious with the increase of the systems size. Additionally, MP2 relative energies of any peptide suffer from the intramolecular basis set superposition error[27-29] whereas this error is negligible when DFT methodologies are used.[30]

Experimental setup.

The experimental setup has been described elsewhere[31]. We obtained GFA from Sigma-Aldrich and used it without further purification. In brief, we prepare samples by applying the neat compound to the surface of a graphite substrate. To bring the molecules into the gas phase, we employ laser desorption using a Nd:YAG laser operating at its fundamental wavelength (1064 nm). The laser is attenuated to 1mJ/cm^2 and focused to a spot approximately 0.5 mm diameter within 2 mm in front of a pulsed nozzle. We translate the sample in order to expose fresh sample to successive laser shots. The nozzle consists of a pulsed valve with a nozzle diameter of 1 mm and a backing pressure of 5 atm. of argon drive gas.

To obtain a resonant two-photon ionization (R2PI) spectrum, we use a frequency doubled dye laser and detect the photo-ions in a time-of-flight mass spectrometer. By monitoring specific mass peaks while varying the two-photon ionization wavelength, we obtain mass selected excitation spectra. We perform double resonance spectroscopy by applying two successive laser pulses separated by a delay of about 200 ns. As a result of this delay we obtain two peaks in the time-of-flight spectrum that can be monitored individually. The first laser pulse serves as an intense "burn" laser, and is scanned over the desired wavelength region, while the delayed laser is used as the "probe" laser, and is fixed on one resonance. The burn laser depletes the ground state and when both lasers are tuned to a resonance of the same conformer, this causes a decrease in the signal of the probe laser. To obtain IR spectra for each conformer, we use IR-UV double resonance spectroscopy by employing an IR laser as the burn laser[32-34]. For this purpose we use an OPO system (LaserVision) pumped by a Nd:YAG laser. The output of the OPO system is 8 mJ/pulse and the bandwidth is 3 cm^{-1}.

Computational details and methods.

1. Molecular dynamics/quenching (MD/Q) technique.

We used the MD/Q technique, described elsewhere,[35] to scan the PES of the GFA tripeptide, employing the self-consistent charge density functional tight-binding method extended by an empirical dispersion term (SCC-DF-TB-D).[36] Typically, the MD/Q technique is confirmed with an empirical potential. In our previous paper[37] we have shown, however, that the PES determined with the AMBER potential differs substantially from that evaluated with the SCC-DF-TB-D method. The SCC-DF-TB-D method is based formally on DFT theory since the equations applied are derived from a second-order expansion of the DFT total energy functional with respect to charge density fluctuations about a given reference density. We have explicitly added an empirical dispersion term to cover the London-type dispersion energy not otherwise included in the parameterization of the model. We have already demonstrated the SCC-DF-TB-D method to be efficient for the screening of the PES of isolated small peptides containing aromatic rings. After scanning the conformational landscape, we sorted all the conformers on the basis of the SCC-DF-TB-D energies and geometries. This procedure reduced the initial set of energy minimized structures to a set of geometrically distinct structures corresponding to all the existing minima in the PES.

2. Ab initio quantum-chemical calculations.

The lowest energy minima (within a relative energy of ~3.5 kcal/mol) obtained from the MD/Q calculations were optimized at the RI[38,39]-MP2/cc-pVDZ[40] level of theory (see Chart 1). Next, the lowest energy conformers from this set (within a relative energy of ~2 kcal/mol) were again recalculated at the RI-MP2/cc-pVTZ level of theory. The MP2/cc-pVTZ calculations are known to provide rather accurate geometries of molecular clusters and we believe that the same will be true for the peptides here investigated. However, reliable geometries obtained at this level are due to a

compensation of errors; the effect of improving the basis set at the MP2 level is compensated by the neglected higher-order correlation effects. We performed RI-MP2/cc-pVQZ[40]//RI-MP2/cc-pVTZ single-point calculations on these geometries and used the extrapolation scheme of Helgaker and co-workers[41] in order to obtain complete basis set (CBS) limit energies ($MP2_{CBS}$). Additionally we added higher-order contributions to the correlation energy beyond the second perturbation order, the $MP2_{CBS}$ energies, by calculating the difference between CCSD(T) and MP2 relative energies (CCSD(T)-MP2) determined with the 6-31G*(0.25) basis set. This correction term is known to be essentially independent of the basis set size, contrary to the MP2 and CCSD(T) energies themselves.[42] We computed theoretical infrared (IR) spectra only for the conformers calculated at the highest level of theory, i.e. CCSD(T)/CBS. We employed scaled harmonic frequencies for the calculation of zero-point vibrational energies (ZPVE), enthalpies, entropies and Gibbs energies (T = 300K) in the context of RR-HO-IG approximation. The scaling factors[43] employed were 0.958, 0.951 and 0.956 for the NH_{ind}, NH_{pep} and OH frequencies, respectively. The latter, was also used for all the mid-IR bands.

3. Resolution of Identity density functional theory augmented with an empirical dispersion term (RI-DFT-D).

The idea behind this method[21] is conceptually straight forward: the DFT theory is improved by adding an empirical term describing the dispersion energy, while maintaining practically the same CPU time requirements. Augmenting the DFT energy by dispersion is not a new concept and it was used for the first time in our previous paper[36] in whch we combined tight-binding DFT energy with empirical London dispersion energy. A van der Waals correction to DFT theory has also been developed by Grimme.[44-46] Essentially, in the RI-DFT-D method, the London dispersion energy is included by a damped pair-potential which has been parameterized against CCSD(T)/CBS results for model complexes containing important non-covalent binding motifs. We performed all the calculations using the TPSS[47] functional which gives results comparable with those of the B3LYP[48] hybrid functional but at a lower computational

cost. We used the Pople 6-311++G(3df,3pd)[49] (abbreviated as LP in this paper) for the geometry optimizations and frequency calculations. We have tested the performance of this procedure for a set of 22 noncovalent complexes containing H-bonded, dispersion-controlled and mixed complexes and the mean-averaged error (with respect to accurate CCSD(T)/CBS values) was the lowest among various WFT and DFT techniques including the MP2/CBS ones. All the thermodynamic properties presented here were calculated under the assumption of the RR-HO-IG approximation. We applied scaling factors of 0.984, 0.976 and 0.988[22] for the OH, NH_{ind} and NH_{pep} frequencies, respectively, with a universal scaling factor of 0.984 for the remaining vibrational modes.

4. M06-2X functional. We used the M06-2X functional of Truhlar[23] in combination with 6-311+G(2df,2p)[49] basis sets for geometry optimizations and single-point energy calculations, respectively. The M06-2X functional belongs to a new generation of hybrid meta-generalized-gradient-approximation exchange–correlation functionals which include an accurate treatment of the London dispersion energy. The method performs very well for predicting noncovalent interactions.

5. Metadynamics

Metadynamics[19,20] is a recently introduced free energy modelling technique. In metadynamics a system is simulated by a standard molecular dynamics simulation to which a history-depended bias potential is added. This bias potential continuously floods free energy basins and thus enhances sampling of configurational space by disfavouring previously explored regions. Moreover, after flooding all basins, this bias potential approximates a free energy surface of the system. A free energy surface calculated by metadynamics is a function of a limited number of collective variables (typically two). Collective variables are geometric parameters that are selected to determine progress of the studied process. The pair of collective variables used in this study were a conformational change and intramolecular hydrogen bond formations, specifically the

Ramachandran φ angle of the alanine residue and the distance, d, between the hydrogen atom of the carboxyl termini group and the oxygen atom of residue *i+1* (see Chart 3).

We performed metadynamics in its direct formulation[50] both at the SCC-DF-TB-D level of theory and using an empirical force field (AMBER 99).[51] For the latter, two sets of RESP (Restricted electrostatic potential fit) charges served as partial atomic charges. The HF/6-31G* RESP charges are the default choice for this force field but are known to be more suitable for the condensed phase calculations and the B3LYP/cc-pVTZ charges provide a more realistic description of isolated molecules. A more detailed discussion about the atomic charges can be found in the results and discussion section. AMBER runs comprised 5 million steps (5 ns). Every 500 steps (0.5 ps) we added a Gaussian hill of 0.05 kcal/mol height and a weight definded by a dihedral angle of 0.3 rad and a distance of 0.6 Å. The metadynamics run at SCC-DF-TB-D level comprised 600.000 steps (600 ps). In this case, every 100 steps (0.1 ps) a Gaussian hill was added. This Gaussian hill was 0.1 kcal/mol in height from 0 to 500 ps and 0.05 kcal/mol in height from 500 to 600 ps. Their widths were the same as for metadynamics using the AMBER force field.

6. Symmetry-Adapted Perturbation Theory combined with DFT (DFT-SAPT).

This work represents a first analysis of the nature of the peptide backbone-aromatic side chain *intramolecular* interaction by means of the symmetry-adapted perturbation theory combined with DFT and implemented using density fitting (DF-DFT-SAPT).[52-57] For this purpose we modelled the isolated peptide by the complex resulting from the splitting of the peptide into the backbone and aromatic side chain interacting fragments (see Figure 4). We added hydrogen atoms *a posteriori* and for the sake of simplicity we later reduced the peptide backbone to the fragment likely interacting with the aromatic side chain (see Figure 4). The conformation and spatial arrangements of the resulting complexes was identical to that obtained at the RI-MP2/cc-pVTZ level of theory for the given isolated peptide conformer.

At the present time, DF-DFT-SAPT is the only methodology providing physically meaningful information about the nature of the intermolecular interaction of molecular systems with up to several dozens of atoms. The reason is that the SAPT intersystem[58] treatment is combined with a DFT description of the subsystems allowing for the study of large molecules. Furthermore, its implementation using the density fitting of two-electron objects[56] drastically reduces the cost of the conventional DFT-SAPT method. In DF-DFT-SAPT, the intermolecular interaction energy is decomposed as the sum of the first order electrostatic ($E_{el}^{(1)}$) and exchange-repulsion ($E_{exch}^{(1)}$) contributions, and the second-order induction ($E_{ind}^{(2)}$), exchange-induction ($E_{exch-ind}^{(2)}$), dispersion ($E_{disp}^{(2)}$) and exchange-dispersion ($E_{exch-disp}^{(2)}$) contributions. Induction, exchange-induction and charge-transfer effects of higher than second order in the intermolecular perturbation operator are estimated from supermolecular Hartree-Fock calculations and denoted as δ(HF).[52] The computational details of the DF-DFT-SAPT calculations here performed are analogous to those described by Jansen et al.[55]

Codes

We determined energies, geometries, harmonic vibrational frequencies and thermodynamic characteristics with RI-MP2 and RI-DFT-D (in our own implementation) methods using the TURBOMOLE 5.8 program package.[59] We performed CCSD(T) and DF-DFT-SAPT calculations with the MOLPRO 2002.1 program[60] and MD/Q simulations with the DFTB+ program. [61] Additionally, we used our own scripts for the selection of the geometrically distinct structures. For the metadynamic calculations with the AMBER force field we used the GROMACS package[62] with a metadynamics extension[50] whereas for the SCC-DF-TB-D metadynamics run, we used our own MD code interfaced to DFTB+ program[61] performing the energy and gradient calculations. Fot the latter case we implemented metadynamics[50] in a formulation identical to the one used in GROMACS.[62] The DFT calculations using the recently introduced M06-2X functional employed QChem 3.1.[23,63]

Results and discussion

Localization of conformers coexisting in the gas phase

MD simulations using empirical force fields, e. g. AMBER, are typically used for the study of multiconformational systems such as peptides. However, atomic charges of a flexible molecule may vary significantly from one conformation to the other consequently affecting the final results. Therefore, in order to assess the applicability of the AMBER force field for the study of peptides, we have calculated the RESP atomic charges for six geometrically distinct conformers out of the 15 most stable conformers in the PES determined at the B3LYP/cc-pVTZ and HF/6-31G* levels of theory (see Tables S1 and S2 in the supplementary information). The first technique (DFT) is used when accurate charges for gas-phase simulations are to be determined while the second technique (HF) is applied for simulations in the water environment.

Tables S1 and S2 reveal a very large dispersion of atomic charges for single conformers. The largest dispersion concerns internal carbon and nitrogen atoms where single conformer charges differ even more than 100% (e.g. C2 in Table S1). But charges at vicinal hydrogen atoms differ dramatically as well. For example, charges on H1 (see Table S1) in various structures vary by +13% and -31%. Evidently, introducing an average charge brings some uncertainty which results in incorrect structural predictions when an empirical potential is used. On the other hand, this finding supports the use of an ab initio procedure for scanning the PES. Such a procedure reduces the uncertainty since the charges are calculated for each structural arrangement.

< Chart 1>

Consequently we investigated the PES of the GFA tripeptide by means of the strategy of calculation shown in Chart 1, namely: implementing MD/Q[35] simulations using tight-binding DFT-D theory[36] followed by accurate quantum chemical calculations. in our previous paper we used a less sophisticated strategy.[37] The present procedure

allows us to localize all the existing minima in the PES, the most stable of which are further recalculated at different ab initio levels of theory. The quality of this step thus clearly affects the quality of all following steps. The number of calculated conformers decreases with the increasing level of theory. The outcome of this sequence of calculations is a set of conformers, which we may expect to include the ones detected experimentally in the gas phase (see Figure 1).

<Figure 1>

Structural analysis.

Figure 1 displays all conformers within a relative energy interval less than 2 kcal/mol and ordered according to the Gibbs energy scale (T = 300K). The reasons why the relative energy interval is based on Gibbs energy scale and not potential energy scale are discussed at the beginning of the next paragraph. Before going into a more detailed analysis of the structural features of the GFA conformers, we would like to point out that the root-mean-square deviations (RMSDs) between the RI-MP2/cc-pVTZ and RI-DFT-D/TPSS/LP geometries is only 0.11Å, meaning that both methods provide almost identical geometries and thus reinforcing the efficacy of the RI-DFT-D method as an adequate tool for the study of larger peptides.[22]

<Chart 2>

The structures shown in Figure 1 can be grouped in different families of conformers, labelled following the Ramachandran terminology[1] as β_L (structures 1, 3, 4, 5, 9 and 10) and γ (structures 6, 7, 8, 11, 12, 15 and 16), since they resemble the β-strands

and γ-turns encountered in proteins.[64] There are still two additional families, designated as 3_{11} (structure 2) and γ-3_{11} (structures 13 and 14). The main structural difference among the families concerns obviously the backbone conformations. In the β strand-like (β_L) structures the peptide backbone is fully extended favouring the $C{=}O_{[i+1]}\cdots HN_{[i+1]}$ interaction (referred to as C_5 conformation; see Chart 2) whereas in the γ-structures the $C{=}O_{[i]}\cdots HN_{[i+2]}$ interaction is formed via a seven atom ring (referred to as C_7 conformation; see Chart 2) involving, the three amino acid residues of the peptide. The γ-3_{11} family shows common structural features (local backbone/backbone interactions) with both, the γ and 3_{11} families, the latter describing a peptide backbone conformation in which the $-CO_2H$ and $-NH_2$ termini groups form an intramolecular H-bond (HOC=O···HNH) involving the 3 residues via an eleven atom ring (C_{11} conformation in Chart 2). The existence of this intramolecular interaction has been reported in proteins[65] and has also been observed for our previously studied tripeptides Phe-Gly-Gly[37] and Trp-Gly-Gly.[43]

In the β_L structures the aromatic side chain is systematically oriented towards the –COOH terminus whereas in the γ structures it is systematically oriented towards the $-NH_2$ terminus. Notice as well that in the γ structures, the $-NH_2$ terminus prefers the orientation where the lone pair electrons of the nitrogen atom are pointing towards the -NH moiety of residue *i+1*, which itself points towards the aromatic side chain, consequently favouring the establishment of a network of weak intramolecular interactions (see e.g. C_7 conformation in Chart 2). In the γ family, the aromatic side chain could never be oriented towards the –COOH terminus since the oxygen atoms of residues *i+1* and *i+2*, and the π cloud will strongly repel each other. There is no β_L structure in which the aromatic ring is oriented towards the $-NH_2$ terminus. The reason for this absence follows from the structures GFA_01 and GFA_06 in Figure 1: when the aromatic side chain is oriented towards the $-NH_2$ terminus, the extended peptide backbone of the β_L structure (e.g. GFA_01) folds into a γ conformation (e. g. GFA_06). It is not clear whether the peptide backbone conformation determines the orientation of the aromatic side chain or whether conversely the aromatic side chain induces the different folded backbone conformations. However, the NH(*i+2*)-aromatic side chain interaction in

combination with successive C_5 (see Chart 2) appears characteristic for the existence of β_L peptide backbone conformations.

There is, also, an alternative classification of the conformers based on the existence of an (C=O)OH···O=C intramolecular H-bond between the hydrogen of the termini carboxyl group and the backbone CO of residue (i+1) (see e.g. C_7 conformation in Chart 2). According to this classification two families of structures exist, designated as CO_2H_{bonded} for all the γ structures and two β_L (GFA_09,10) and as CO_2H_{free} for the remaining structures. Such intramolecular interaction is interesting for various reasons. To start with, it is responsible for the folding of the backbone into a C_7 conformation suggesting the possible appearance of consecutive γ-turns if the peptide backbone would be extended by additional residues (see Chart 2). The existence of multiple γ-turns in a peptide backbone has been addressed in the literature.[66,67] More interestingly and analogous to the case of Phe-Gly-Gly,[37] Trp-Gly[43,68,69] and Trp-Gly-Gly,[43,68,69] we observed none of the predicted CO_2H_{bonded} structures experimentally. This quite intriguing observation motivated us to review our calculations on the free energy surface. This normally forms the least reliable step of the theoretical procedure because usually free energy calculations are based on the RR-HO-IG approximation which limits the level of the entire theoretical procedure. However, in the present paper we employed the metadynamics procedure based on tight-binding DFT-D which goes beyond the harmonic approximation.

Stability of the conformers.

According to the H-bond pattern presented by the conformers shown in Figure 1, one would expect that the γ structures will be followed in stability by the β_L CO_2H_{bonded}, the γ-3_{11}, 3_{11} and β_L CO_2H_{free} structures since the higher number of H-bonds would be expected to correlate with more stable structures. This hypothesis is confirmed by the relative electronic energies obtained at the RI-DFT-D/TPSS/LP level of theory (see column 8 in Table 1) and verified as well against CCSD(T)/CBS benchmark data (see column 2 in Table 1), having a mean unsigned error of the RI-DFT-D with respect to

CCSD(T) relative energies of 1.26 kcal/mol. The absolute values of the relative energies at these two levels of theory are somewhat different, however the trends are the same. First and significantly, both methods predict the same global minimum structure (GFA_15). Secondly, both predict CO_2H_{bonded} structures to be more stable than CO_2H_{free} conformers. Furthermore, the ordering of structures within the CO_2H_{bonded} family at the RI-DFT-D/TPSS/LP level of theory matches pretty well, except for the GFA_16 conformer, with that of the benchmark data. The CO_2H_{free} subfamily exhibits larger disagreements although both methods agree in predicting the structures with a folded backbone (e.g. GFA_02) to be more stable than those with an extended one (e.g. GFA_01).

< Table 1>

Column 6 in Table 1 lists the single-point energies obtained at the M06-2X/6-311+G(2df,2dp) level of theory for the RI-MP2/cc-pVTZ geometries. A first conclusion that can be drawn from these data is that the global minimum at the DFT level of theory, i.e. GFA_16 (see column 6, Table 1) is not the same as the global minimum predicted at the benchmark level of theory, i. e. GFA_15 (see column 2, Table 1). The difference in energy between GFA_16 (global DFT minimum) and GFA_15 (benchmark data minimum) at the M06-2X/6-311+G(2df,2dp) level is 1.54 kcal/mol. There is also a disagreement in the order of structures in the two sets. According to the benchmark data calculations the CO_2H_{bonded} family of structures is more stable than the CO_2H_{free} family. In the case of the M06-2X functional, this order is not that well established and structures from different families are interspersed. Furthermore, GFA_01, the least stable conformer in the benchmark database, is in the sixth position in the ranking of energies calculated using the M06-2X functional. The same situation occurs when looking at structures GFA_10 and GFA_11, occupying the third and sixth position at the benchmark level, respectively (column 2 of Table 1) and being the two least stable structures in the DFT scale (column 6 in Table 1).

The level of calculations performed is very high and we can thus be confident about the quality of the PES obtained. This means that the lowest energy structures should co-exist and should thus be detected experimentally at very low temperatures (the calculations correspond to 0 K). At very low temperatures the entropy term in the expression for the Gibbs energy is small and can be neglected against the enthalpy (energy) term. However, the spectroscopic measurements are done on a distribution of structures established right after the peptide is laser desorbed, implying that free energy and not enthalpy (energy) will be controlling the final relative population of these structures. With this assumption, the final selection of conformers should be based on Gibbs energies (T = 300K) instead of electronic energies. In other words, zero-point vibrational energies (ZPVE), thermal corrections to the enthalpy and entropies should be taken into account in the calculation of the relative stabilities of the conformers. The population in the beam is not known, however one possible assumption is that the population distribution, originated before the expansion taks place, is preserved to a large extent during the relatively fast supersonic cooling.[70] In other words, although the cooling is a non-equilibrium process, the final conformations may still at least partly reflect the original thermodynamic distribution. In this simplified model we can roughly estimate the populations according to a Maxwell-Boltzman distribution.

Table 1 shows the thermodynamic functions ΔH_0 and ΔG, and populations at 300K for the studied conformers. The inclusion of the ZPVE (i.e. passing from ΔE to ΔH_0), reduces the energy interval, which is covered by these structures, from 2.14 and 4.08 kcal/mol to 0.62 and 0.68 kcal/mol at the CCSD(T)/CBS and RI-DFT-D/TPSS/LP levels of theory, respectively. Furthermore, it significantly changes the order of the structures. Unlike in the ΔE scale where the CO_2H_{bonded} structures are the most stable ones, in the ΔH_0 scale, the CO_2H_{free} structures are favoured (both at the CCSD(T)/CBS and RI-DFT-D/TPSS/LP level of theory).

Neither the inclusion of the thermal correction to the enthalpy nor the inclusion of entropic contributions alter the order of conformers any further and thus, the CO_2H_{free} structures remain as the most stable ones in the FES. Conformers with a larger number of intramolecular H-bonds have a higher relative order within the backbone conformation,

and as expected, are less affected by the entropic contributions. One effect of the inclusion of the entropic contribution is the increase of the energy differences between conformers, now lying within an interval of approximately 3 kcal/mol at both, the CCSD(T)/CBS and RI-DFT-D/TPSS/LP levels of theory (the mean unsigned error of the relative Gibbs energies between the RI-DFT-D and CCSD(T) method is 0.5 kcal/mol). We have used these Gibbs relative energies for the calculation of the relative population of structures according to a Maxwell-Boltzmann distribution at T=300K which are listed in Table 1. In essence five conformers (GFA_01, 02, 03, 04 and 05) are entropically favored (i.e. have lower relative Gibbs energies) over the others. Namely, four β_L and the 3_{11} structures or according to our second structural classification, five out of the seven CO_2H_{free} structures.

Free energy surface analysis by metadynamics.

Gibbs energies and populations obtained from ab initio quantum chemical calculations assuming a RR-HO-IG approximation are only accurate to some extent. Indeed, a population analysis based on MD is more robust, because it samples the whole conformational space and goes beyond the harmonic approximation. However, the SCC-DF-TB-D trajectories ran in this work are too short to provide reliable thermodynamic data and as discussed above the use of empirical force fields is not recommendable for the study of isolated small peptides.

In order to overcome these limitations and to make sure that the conformational landscape obtained by the combination of MD/Q simulations with high-level correlated ab initio quantum chemical calculations including the RR-HO-IG approximation for determining the thermodynamic characteristics (MD/Q+QM) is correct, we have employed the metadynamics algorithm to independently explore the free energy surface of GFA tripeptide. Metadynamic calculations yield two-dimensional free energy surfaces from shorter simulations than standard MD simulations. The reason is that it allows controlled sampling of specific structural features and thus the simulation time needed is significantly reduced. For the present case, the two selected coordinates (see Chart 3)

were chosen to distinguish between the CO_2H_{free} and CO_2H_{bonded} families. We performed three metadynamic calculations. One at the SCC-DF-TB-D level of theory and the remaining two using the AMBER force field with different sets of RESP charges (HF/6-31G* and B3LYP/cc-pVTZ). We have pioneered the implementation of the DFTB+ code into metadynamics and this is the first report of this kind of simulation applied to a peptide at this level of theory. Furthermore these calculations using the AMBER force field in combination with metadynamics serve the following two purposes: a) to analyze the influence that the set of charges has in the AMBER results; and b) to compare the performance of the AMBER force field against the tight-binding DFT-D method. Notice that in all the simulations, numerous transitions between conformers were observed, which confirms the good sampling of the FES. In each simulation, the flooding potential reached a converged level at which the results were read.

< Figure 2>

Figure 2(a) visualizes the SCC-DF-TB-D free energy surface as a map with isoenergetic contours. The minima found from the MD/Q+QM calculations are projected on top of this map (white points) for the shake of comparison. Additionally, the free energies of the minima were averaged over the converged part of the simulation and subsequently the error (measured as 95% confidence interval) was estimated (see Figure 2(b)). From the analysis of Figure 2(a) it can be concluded that both FESs -the one obtained by metadynamics and the MD/Q+QM- are in good agreement. This finding is of key importance since it indicates that anharmonic effects are not playing a decisive role for the present conformers. In fact, in both free energy surfaces the CO_2H_{free} and CO_2H_{bonded} families exist with comparable stability (see below). Structure GFA_16 and GFA_14 have very different φ values (see Chart 3 for the definition of φ) from those in the other members of their corresponding families and consequently they appear in a different region of the contour map. Notice as well, that there is no minimum for structures GFA_04, GFA_05 and GFA_13 on the map. However, this is due to the

resolution of the free energy surface rather than to failure of the method. Most importantly the two independent methods of identifying the most stable conformations of the peptide at the free energy surface comparable results.

Regarding the order of stabilities of the conformers it should be mentioned that one point on the 2D surface corresponds to more structures differing in other structural motifs than those described by coordinates selected for metadynamics. For instance, structures GFA_06 and GFA_09 (see Figure 1) correspond to the CO_2H_{bonded} family, but GFA_06 is a γ structure whereas GFA_09 is a β_L structure. The resulting free energy should be thermodynamic average of these structures. From the analysis of Figure 2(b) it can be concluded that the best overall agreement with the quantum chemical Gibbs energies was achieved at the SCC-DF-TB-D level of theory, although in our simulation it overestimates hydrogen bonding by about 3 kcal/mol. This is in contrast with normal behaviour of SCC-DF-TB-D, which tends to underestimate intersystem hydrogen bonds.[71] This can be at least partially attributed to an artifact of the simulation, because the preference of non H-bonded structures is possible within given error bars (Figure 2(b)).

Similar free energy surfaces were evaluated using the AMBER force field and two different sets of charges (HF/6-31G* and B3LYP/cc-pVTZ) for the sake of comparison. The contour maps of these FES can be found in the supplementary information (see Figure S1) and the free energies of the minima are listed in Figure 2(b). From the data in Figure 2(b), it is clear that the force field using the B3LYP/cc-pVTZ charges underestimates the hydrogen bonding whereas using HF/6-31G* charges provides the best description from the potentials we tested. More importantly, AMBER results are strongly biased towards negative values of the dihedral angle φ and thus, the procedure cannot be recommended for the evaluation of thermodynamic characteristics. Similar behaviour of the AMBER ff99 is discussed in Ref. [72].

Comparison with the experiment.

<Figure 3>

Figure 3 shows the ground state IR spectra measured for GFA tripeptide in the 3200 – 3700 cm^{-1} region. We obtained each of these IR-UV hole burning traces by setting the UV probe wavelength at the origin of a different one of the four conformers in the R2PI spectrum. Scaled theoretical spectra of the assigned structures (see below) calculated using both RI-MP2 and RI-DFT-D methods appear as well. Table S3 and Table S4 of the Supporting Information list the exact values of the calculated and experimental frequencies. According to the experimental data four different conformers within the CO_2H_{free} family, characterised by a free OH stretch frequency in the spectra, co-exist in the gas-phase. The theoretical data predict a larger number of structures than the number we observe experimentally. The same phenomenon has previously been reported for several other peptides.[70,73,74] This raises the question how to reconcile the more complicated conformational landscape predicted theoretically with the apparently 'simpler' conformational picture derived experimentally.

One possible explanation is that the experimental data could be incomplete for which there could be several reasons. Oscillator strengths or Frank-Condon factors for certain conformers might be too small to permit their measurement. It is possible to miss conformations when their UV spectrum is shifted outside the experimental range. It is also possible to miss structures if their ionisation potential is more than twice the photon energy used. However, it is not obvious why any of these conditions would apply selectively to any of the calculated conformations. The same holds for the assumption that collisional relaxation in the free jet expansions selects specific conformers.

Another intriguing possibility why we might not observe specific structures in our R2PI experiments is a short excited state lifetime. A sub-picosecond excited state lifetime could preclude detection in our experiment, because we employ two photon ionization

with nanosecond laser pulses. For nucleobases a number of excited state calculations suggest that rapid internal conversion (IC) can be highly structure selective. Several groups have proposed models in which IC takes place *via* conical intersections.[75-80] Whether or not these intersections have barriers depends very sensitively on molecular structure, which can lead to lifetimes that can differ by orders of magnitude between fairly similar structures. The failure to experimentally observe selected tautomers and cluster structures appears to be consistent with these models. One of several proposed IC pathways involves πσ* states with motion along an H-bond N-H coordinate. Sobolewski and Domcke have recently proposed that such excited state dynamics can also occur in peptides.[81] The predicted structures that go unobserved in our experiment all involve an internal hydrogen bond of CO_2H_{bonded}. As previously reported, for the case of Phe-Gly-Gly, Trp-Gly and Trp-Gly-Gly peptides, the structures containing an (C=O)OH···O=C intramolecular H-bond were not observed experimentally. We are currently undertaking experiments to see if we can observe the "missing" structures by using femtosecond ionisation and by bypassing the S1 state with single photon ionization.

Our theoretical calculations suggest the existence of four different families in the PES (or FES): β_L, 3_{11}, γ and γ -3_{11}, two of which, β_L and 3_{11}, are predicted to be entropically favoured, that is to be more stable in the FES.

(a) *β_L family of structures:* In a β_L structure (see Figure 1), the peptide backbone is extended so five IR lines should be observed in the 3200-3700 cm^{-1} spectral region corresponding to the carboxyl O-H stretch (OH), the amino NH_2(S), symmetric, and NH_2(A), antisymmetric, stretches and the peptide N-H stretch (NH_{pep}) vibrations. Our conformational search, suggest the existence of four very stable structures within the β_L family (GFA_01, 03, 04, 05) which themselves can be clustered into two subfamilies according to the orientation of the $–NH_2$ and CO_2H terminal groups. However, the classification of these four structures is not fully straightforward since it depends on the criteria of selection. On the one hand, we could consider structures GFA_01 and GFA_03, and consequently GFA_04 and GFA_05, to be members of the same family showing different orientations of the $–NH_2$ terminal group and similar orientation of the CO_2H termini group. Alternatively we could consider structures GFA_01 and GFA_05,

and consequently GFA_03 and GFA_04, to be members of the same family showing different orientations of the CO_2H terminal group and similar orientation of the $–NH_2$ terminal group. What seems to be clear is that there are two β_L subfamilies distinguishable in the spectroscopic record, since two of the experimental spectra (spectrum (1) and (2) in Figure 3) nicely match those calculated for the GFA_01, 03, 04 and 05 β_L structures. We can not determine whether the experimentally reported spectra result from the contribution of one or two β_L conformers and which of the β_L subfamilies is represented by which of the spectra.

(b) *3_{11} family of structures.* The assignment of the spectra of the GFA_02 structure, representing the *3_{11}* family, is more straightforward. From inspection of Figure 3 it can be clearly seen that its scaled theoretical spectrum agrees well with the experimental spectrum (3).

(c) *The γ family of structures*. We have observed in the structural analysis that all the *γ* structures belong to the CO_2H_{bonded} family. Thus, all of these structures show a spectral line in the 3200 cm^{-1} spectral region (see Tables S3 and S4) resulting from the involvement of the OH group in an intramolecular H-bond. Consequently, none match any of the experimental structures. The same is true for the GFA_09 and 10 β_L structures.

After excluding structures GFA_06 to GFA_12, the spectrum of the next conformer in the Gibbs energy ranking is GFA_13. The frequencies for this structure agree quite well with spectrum (4) of Figure 3. Two observations should be made here. First, GFA_13 belongs to a new family of conformers with a different conformational peptide backbone than that for the β_L and *3_{11}* families of structures. Second, there is a second member of the *γ-3_{11}* family (structure GFA_14) which we don't observe experimentally (see Table S3 and S4 for its spectroscopic data) but which is equally populated to structure GFA_13.

Analysis of the nature of the peptide backbone-aromatic side chain interaction.

Backbone-aromatic (Ar) side chain interactions affect the stability of peptide conformers in a number of ways.[6,8,9,13,14,16,66,82] In general, it appears that for isolated peptides containing aromatic side chains, β_L structures with an Ar(*i+1*)-NH(*i+2*) interaction are more stable than γ structures with an Ar(*i+1*)-NH(*i+1*) interaction, whereas the opposite is true for peptides without a residue of aromatic character. This propensity has been beautifully illustrated in the comparison of the N-Ac-Ala-NH_2, N-Ac-Gly-NH_2 and N-Ac-Phe-NH_2 (NAPA)[9,82] related species. Chin *et al*[9] have shown that these systems with capped end groups adopt both, γ and β_L(a) peptide backbone conformations and that their relative stability (γ structures more stable than β_L(a) or the other way around) depends on the formation of a N-H(*i+2*)$\cdots\pi$ interaction. Additionally, for the NAPA system, the authors described the different types of intramolecular interactions formed within the molecule, which they further characterized by orbital population and Atoms-In-Molecules analysis. In these capped model peptides, none of the intramolecular interactions involving unprotected termini can occur, such as the HNH(*i*)-OCOH(*i+2*) which is prevalent in the GFA tripeptide with unprotected end-groups. Yet, the β_L(a) backbone conformation is the preferred structural motif both in the uncapped peptide and in the capped model system.

<Figure 4>

In the C_7 backbone conformation of the γ structures as well as the pseudo-C_7 conformation of the 3_{11} structure (see Chart 2) the -NH moiety of residue *i+1* is pointing towards the aromatic side chain. However, in the β_L structures, the NH moiety involved in the N-H$\cdots\pi$ interaction belongs to residue *i+2* (instead of residue *i+1*) and lies parallel to the aromatic side chain. We wonder then if the nature of the backbone-aromatic side chain interaction is of the same character for these two very different geometrical rearrangements and which is the driving force, if any, of these interactions. We have modelled different representative conformations by a peptide backbone fragment –

benzene intermolecular complex (see Figure 4 and Computational details and Method section for a description of the models) and we have performed a qualitative analysis based on the importance of the different components of the interaction energy provided by DF-DFT-SAPT (see Table S5 in the Supporting information). In the case of structure GFA_02, we had to split the peptide backbone fragment into two subfragments in order to avoid an artificial repulsion between the components originating from the proximity of the *a posteriori* added hydrogen to the benzene ring.

The stick spectrum of Figure 4 shows that the dispersion energy, $E_{disp}^{(2)}$, is the largest attractive contribution to the interaction energy. The importance of the electrostatic contribution ($E_{el}^{(1)}$) varies slightly depending on the directionality of the –NH moiety: The more pointing the –NH, the higher the $E_{el}^{(1)}$ component. This result is in agreement with the conclusion by Tsuzuki et al.[11] for the benzene-ammonia model system that the electrostatic force (dipole(NH)- quadrupole(benzene)) dominates the directionality of the NH···π interactions. Finally, the induction contribution ($E_{ind}^{(2)}$) plays a minor -though not negligible- role in the interaction and the repulsion energy –mainly coming from the $E_{exch}^{(1)}$ exchange contribution- has a significant influence on the equilibrium of the forces. An overall conclusion that can be obtained from the SAPT analysis is, the important role played by the dispersion energy ($E_{disp}^{(2)}$) in the peptide backbone-aromatic side chain interaction. This conclusion supports our observation that the DFT methodology, which does not cover the London dispersion energy, insufficiently describes peptides of aromatic character.

Conclusions.

Localizing the different conformations co-existing in the gas phase of a peptide requires exploration of the free energy surface of the system. Part of the conformers predicted to be more stable for the GFA tripeptide according to the Gibbs energies by statistical thermodynamics and metadynamics calculations agree well with those observed experimentally. However, there is an additional family reported theoretically

and not observed experimentally. One possible explanation is a short excited state lifetime in the structures which we failed to observe experimentally.

A proper scan of the FES requires the use of a non-empirical method. The AMBER empirical force field fails mainly due to a large variety of atomic charges for individual conformers. Additionally, we can not fully disregard the possibility of attributing the failure of AMBER to an inaccurate fitting to the dihedral term during the force field development. The FES obtained by means of the combination of MD/Q simulations using the tight-binding DFT-D method with high-level correlated ab initio quantum chemical calculations followed by statistical thermodynamics RR-HO-IG calculations is confirmed by the FES obtained independently with the metadynamics calculations based on the tight-binding DFT-D method. This proves both methodologies to be suitable for the study of isolated small peptides.

Metadynamics is a fast and convenient tool modelling the free energy surface of a peptide. However, in combination with the AMBER force field the method provides inaccurate results originating in the failure of AMBER and not in the metadynamics method itself. The use of metadynamics in combination with tight-binding DFT-D is far more recommendable. The use of metadynamics demands a good knowledge of the inherent behaviour of the system under study since the data obtained are largely dependent on the variables chosen to scan the FES. Indeed, relevant structural information can be hidden if the selection of variables is not appropriate.

For the electronic energies and geometries, the TPSS functional augmented with a dispersion term (TPSS-D) provides reasonable results in comparison with the benchmark data at the CCSD(T)/CBS level of theory. However, in case of the M06-2X functional the performance is not that satisfactory probably due to the inaccurate description of the long-range interactions provided by the functional.

The most stable conformers of the GFA tripeptide can be clustered into four families according to the conformational preferences of the peptide backbone. The backbone arrangement of two of these families resembles the β-strands and γ-turns

encountered in analogue capped peptides and in proteins. β_L structures are stabilized by successive C_5 motifs in combination with NH(i+2)···aromatic side chain interactions whereas the γ structures are stabilized by C_7 conformations and a H-bond network involving the amino termini group, the NH(i+1) residue and the aromatic side chain. As for the nature of the backbone/side chain interactions, the dispersion energy is proven to play a relevant role.

We did not experimentally observe the predicted family of γ structures with hydrogen bonded COOH terminal group and we are further exploring the reasons for this intriguing discrepancy.

Acknowledgments

This work was supported by Grant No. A400550510 and LC512 from the Grant Agency of the Academy of Sciences of the Czech Republic and MSMT of the Czech Republic; it was also part of the research project No. Z40550506. A portion of the research described in this paper was performed in the Environmental Molecular Sciences Laboratory, a national scientific user facility sponsored by the Department of Energy's Office of Biological and Environmental Research and located at Pacific Northwest National Laboratory. The research done by V. Spiwok was supported by the Czech Ministry of Education (MSM6046137305). The experimental work is based upon work supported by National Science Foundation (CHE-0615401)

Supporting Information Available:

Tables S1 and S2 containing B3LYP/cc-pVTZ and HF/6-31G* RESP charges, respectively. Tables S3 and S4 containing experimental and scaled theoretical (RI-MP2/cc-pVDZ and RI-DFT-D/TPSS/LP) vibrational frequencies. Table S5 containing the energy contributions to the interaction energy as calculated with DF-DFT-SAPT. Chart S1 with the atoms numbering of Tables S1 and S2. Figure S2 with contour maps obtained using metadynamics in combination with AMBER. This material is available free of charge via the Internet at http://pubs.acs.org.

Figure Captions

Chart 1. Strategy of calculation used for: a) scanning the PES of GFA tripeptide; b) localization of the most stable minima in it and c) calculation of the thermodynamic properties.

Chart 2. Nomenclature definition.

Chart 3. Definition of the collective variables for the metadynamics study.

Figure 1. RI-MP2/cc-pVTZ geometries for the 16 most stable structures of Gly-Phe-Ala tripeptide. The stability of the individual conformers decreases from left to right. The structural family to which conformer belongs is included in the upper left corner.

Figure 2. a) Free energy surface calculated using metadynamics at the SCC-DF-TB-D level of theory. Collective variables are described in text. Free energy minima obtained using MD/Q+QM are illustrated as points labelled according to Figure 1. Distances are given in Å and dihedral angle in degrees; b) free energies (kcal/mol) calculated using metadynamics combined with tight-binding DFT-D and AMBER empirical force field with either HF/6-31G* (AMBER+HF) or B3LYP/cc-pVTZ (AMBER+DFT) set of charges. Labelling according to Figure 1. The energy scale corresponds to the quantum chemical Gibbs energy (see Table 1). CO_2H_{free} structures 1 to 3 were set as zero.

Figure 3. IR ground state experimental spectra of the Gly-Phe-Ala tripeptide. Schematic scaled harmonic spectra at the RI-MP2/cc-pVDZ (dark bars) and RI-DFT-D/TPSS/LP (light bars) levels of theory are also included for comparison.

Figure 4. Intermolecular complexes modeling backbone–aromatic side chain interactions in the GFA conformers. All distances are given in Å. The different components of the interaction energy of representative structures are illustrated in bar diagrams

Reference List

1. C.Branden; J.Tooze *Introduction to Protein Structure;* New York, 1999.

2. Steiner, T.; Koellner, G. *J. Mol. Biol.* **2001,** *305* (3), 535-557.

3. Burley, S. K.; Petsko, G. *Febs Lett.* **1986,** *203* (2), 139-143.

4. Levitt, M.; Perutz, M. F. *J. Mol. Biol.* **1988,** *201* (4), 751-754.

5. Steiner, T. *Angew. Chem.-Int. Edit.* **2002,** *41* (1), 48-76.

6. Toth, G.; Watts, C. R.; Murphy, R. F.; Lovas, S. *PROTEINS* **2001,** *43* (4), 373-381.

7. Palermo, N. Y.; Csontos, J.; Owen, M. C.; Murphy, R. F.; Lovas, S. *J. Comput. Chem.* **2007,** *28* (7), 1208-1214.

8. Toth, G.; Murphy, R. F.; Lovas, S. *J. Am. Chem. Soc.* **2001,** *123* (47), 11782-11790.

9. Chin, W.; Mons, M.; Dognon, J. P.; Mirasol, R.; Chass, G.; Dimicoli, I.; Piuzzi, F.; Butz, P.; Tardivel, B.; Compagnon, I.; von Helden, G.; Meijer, G. *J. Phys. Chem. A* **2005,** *109* (24), 5281-5288.

10. Rodham, D. A.; Suzuki, S.; Suenram, R. D.; Lovas, F. J.; Dasgupta, S.; Goddard, W. A.; Blake, G. A. *Nature* **1993,** *362* (6422), 735-737.

11. Tsuzuki, S.; Honda, K.; Uchimaru, T.; Mikami, M.; Tanabe, K. *J. Am. Chem. Soc.* **2000,** *122* (46), 11450-11458.

12. Bendova, L.; Jurecka, P.; Hobza, P.; Vondrasek, J. *J. Phys. Chem. B* **2007,** *111* (33), 9975-9979.

13. Duan, G.; Smith, V. H.; Weaver, D. F. *J. Phys. Chem. A* **2000,** *104* (19), 4521-4532.

14. Duan, G. L.; Smith, V. H.; Weaver, D. F. *Chem. Phys. Lett.* **1999,** *310* (3-4), 323-332.

15. Cheng, J.; Kang, C.; Zhu, W.; Luo, X.; Puah, C. M.; Chen, K.; Shen, J.; Jiang, H. *J. Org. Chem.* **2003,** *68* (19), 7490-7495.

16. Flocco, M. M.; Mowbray, S. L. *J. Mol. Biol.* **1994,** *235* (2), 709-717.

17. Mitchell, J. B. O.; Nandi, C. L.; Mcdonald, I. K.; Thornton, J. M.; Price, S. L. *J. Mol. Biol.* **1994,** *239* (2), 315-331.

18. Worth, G. A.; Wade, R. C. *J. Phys. Chem.* **1995,** *99* (48), 17473-17482.

19. Iannuzzi, M.; Laio, A.; Parrinello, M. *Phys. Rev. Lett.* **2003,** *90* (23).

20. Laio, A.; Parrinello, M. *PNAS* **2002,** *99* (20), 12562-12566.

21. Jurecka, P.; Cerny, J.; Hobza, P.; Salahub, D. R. *J. Comput. Chem.* **2007,** *28* (2), 555-569.

22. Cerny, J.; Jurecka, P.; Hobza, P.; Valdes, H. *J. Phys. Chem. A* **2007,** *111* (6), 1146-1154.

23. Zhao, Y.; Truhlar, D. G. *Theor. Chem. Acc.,* D.O.I.: 10.1007/s00214-007-0310-x

24. Dabkowska, I.; Gonzalez, H. V.; Jurecka, P.; Hobza, P. *J. Phys. Chem. A* **2005,** *109* (6), 1131-1136.

25. Tsuzuki, S.; Luthi, H. P. *J. Chem. Phys.* **2001,** *114* (9), 3949-3957.

26. Wu, X.; Vargas, M. C.; Nayak, S.; Lotrich, V.; Scoles, G. *J. Chem. Phys.* **2001,** *115* (19), 8748-8757.

27. Holroyd, L. F.; van Mourik, T. *Chem. Phys. Lett.* **2007,** *442* (1-3), 42-46.

28. Toroz, D.; van Mourik, T. *Mol. Phys.* **2006,** *104* (4), 559-570.

29. van Mourik, T.; Karamertzanis, P. G.; Price, S. L. *J. Phys. Chem. A* **2006,** *110* (1), 8-12.

30. Valdes, H.; Klusak, V.; Pitonak, M.; Exner, O.; Stary, I.; Hobza, P.; Rulisek, L. *J. Comput. Chem.* D.O.I.: 10.1002/jcc.

31. Meijer, G.; de Vries, M. S.; Hunziker, H. E.; Wendt, H. R. Appl. Phys. B-Lasers Opt. **1990,** *51* (6), 395-403.

32. Kim, W.; Schaeffer, M. W.; Lee, S.; Chung, J. S.; Felker, P. M. *J. Chem. Phys.* **1999,** *110* (23), 11264-11276.

33. Pribble, R. N.; Zwier, T. S. *Faraday Discuss.* **1994,** (97), 229-241.

34. Schmitt, M.; Muller, H.; Kleinermanns, K. *Chem. Phys. Lett.* **1994,** *218* (3), 246-248.

35. Ryjacek, F.; Engkvist, O.; Vacek, J.; Kratochvil, M.; Hobza, P. *J. Phys. Chem. A* **2001,** *105* (7), 1197-1202.

36. Elstner, M.; Hobza, P.; Frauenheim, T.; Suhai, S.; Kaxiras, E. *J. Chem. Phys.* **2001,** *114* (12), 5149-5155.

37. Reha, D.; Valdes, H.; Vondrasek, J.; Hobza, P.; Abu-Riziq, A.; Crews, B.; de Vries, M. S. *Chem.-Eur. J.* **2005,** *11* (23), 6803-6817.

38. Eichkorn, K.; Treutler, O.; Ohm, H.; Haser, M.; Ahlrichs, R. *Chem. Phys. Lett.* **1995,** *240* (4), 283-289.

39. Eichkorn, K.; Weigend, F.; Treutler, O.; Ahlrichs, R. *Theor. Chem. Acc.* **1997,** *97* (1-4), 119-124.

40. Kendall, R. A.; Dunning, T. H.; Harrison, R. J. *J. Chem. Phys.* **1992,** *96* (9), 6796-6806.

41. Halkier, A.; Helgaker, T.; Jorgensen, P.; Klopper, W.; Koch, H.; Olsen, J.; Wilson, A. K. *Chem. Phys. Lett.* **1998,** *286* (3-4), 243-252.

42. Jurecka, P.; Hobza, P. *Chem. Phys. Lett.* **2002,** *365* (1-2), 89-94.

43. Valdes, H.; Reha, D.; Hobza, P. *J. Phys. Chem. B* **2006,** *110* (12), 6385-6396.

44. Antony, J.; Grimme, S. *Phys. Chem. Chem. Phys.* **2006,** *8* (45), 5287-5293.

45. Grimme, S. *J. Comput. Chem.* **2004,** *25* (12), 1463-1473.

46. Grimme, S. *J. Comput. Chem.* **2006,** *27* (15), 1787-1799.

47. Tao, J. M.; Perdew, J. P.; Staroverov, V. N.; Scuseria, G. E. *Phys. Rev. Lett.* **2003,** *91* (14).

48. Becke, A. D. *Phys. Rev. A* **1988,** *38* (6), 3098-3100.

49. Hehre, W. J.; Radom, L.; Schleyer, P. v. R.; Pople, J. A. *Ab InitioMolecular Orbital Theory;* New York, 1986.

50. Piana, S.; Laio, A. *J. Phys. Chem. B* **2007,** *111* (17), 4553-4559.

51. Wang, J. M.; Cieplak, P.; Kollman, P. A. *J. Comput. Chem.* **2000,** *21* (12), 1049-1074.

52. Hesselmann, A.; Jansen, G. *Chem. Phys. Lett.* **2002,** *357* (5-6), 464-470.

53. Hesselmann, A.; Jansen, G. *Chem. Phys. Lett.* **2002,** *362* (3-4), 319-325.

54. Hesselmann, A.; Jansen, G. *Chem. Phys. Lett.* **2003,** *367* (5-6), 778-784.

55. Hesselmann, A.; Jansen, G. *Phys. Chem. Chem. Phys.* **2003,** *5* (22), 5010-5014.

56. Hesselmann, A.; Jansen, G.; Schutz, M. *J. Chem. Phys.* **2005,** *122* (1).

57. Jansen, G.; Hesselmann, A. *J. Phys. Chem. A* **2001,** *105* (49), 11156-11157.

58. Jeziorski, B.; Moszynski, R.; Szalewicz, K. *Chem. Rev.* **1994,** *94* (7), 1887-1930.

59. Ahlrichs, R.; Bar, M.; Haser, M.; Horn, H.; Kolmel, C. *Chem. Phys. Lett.* **1989,** *162* (3), 165-169.

60. MOLPRO is a package of ab initio programs written by Werner, H.-J. et al.

61. Aradi, B.; Hourahine, B.; Frauenheim, T. *J. Phys. Chem. A* **2007,** *111* (26), 5678-5684.

62. van der Spoel, D.; Lindahl, E.; Hess, B.; Groenhof, G.; Mark, A. E.; Berendsen, H. J. C. *J. Comput. Chem.* **2005,** *26* (16), 1701-1718.

63. Shao, Y. et al. *Phys. Chem. Chem. Phys.* **2006,** *8* (27), 3172-3191.

64. Chou, K. C. *Anal. Biochem.* **2000,** *286* (1), 1-16.

65. Lansbergen, G.; Komarova, Y.; Modesti, M.; Wyman, C.; Hoogenraad, C. C.; Goodson, H. V.; Lemaitre, R. P.; Drechsel, D. N.; van Munster, E.; Gadella, T. W. J.; Grosveld, F.; Galjart, N.; Borisy, G. G.; Akhmanova, A. *J. Cell Biol.* **2004,** *166* (7), 1003-1014.

66. Chin, W.; Mons, M.; Dognon, J. P.; Piuzzi, F.; Tardivel, B.; Dimicoli, I. C *Phys. Chem. Chem. Phys.* **2004,** *6* (10), 2700-2709.

67. Fricke, H.; fer, G.; Schrader, T.; Gerhards, M. *Phys. Chem. Chem. Phys.* **2007,** *9* (32), 4592-4597.

68. Bakker, J. M.; Plutzer, C.; Hunig, I.; Haber, T.; Compagnon, I.; von Helden, G.; Meijer, G.; Kleinermanns, K. *ChemPhysChem* **2005,** *6* (1), 120-128.

69. Hunig, I.; Kleinermanns, K. *Phys. Chem. Chem. Phys.* **2004,** *6* (10), 2650-2658.

70. Robertson, E. G.; Simons, J. P. *Phys. Chem. Chem. Phys.* **2001,** *3* (1), 1-18.

71. Kabelac, M.; Valdes, H.; Sherer, E. C.; Cramer, C. J.; Hobza, P. *Phys. Chem. Chem. Phys.* **2007,** *9* (36), 5000-5008.

72. Lwin, T. Z.; Luo, R. *Protein Sci.* **2006,** *15* (11), 2642-2655.

73. Godfrey, P. D.; Brown, R. D. P. *J. Am. Chem. Soc.* **1998,** *120* (41), 10724-10732.

74. Sanz, M. E.; Cortijo, V.; Caminati, W.; Lopez, J. C.; Alonso, J. L. *Chem.-Eur. J.* **2006,** *12* (9), 2564-2570.

75. Kistler, K. A.; Matsika, S. *J. Phys. Chem. A* **2007,** *111* (35), 8708-8716.

76. Kistler, K. A.; Matsika, S. *J. Phys. Chem. A* **2007,** *111* (14), 2650-2661.

77. Marian, C. M. *J. Phys. Chem. A* **2007,** *111* (8), 1545-1553.

78. Perun, S.; Sobolewski, A. L.; Domcke, W. *Chem. Phys.* **2005,** *313* (1-3), 107-112.

79. Seefeld, K. A.; Plutzer, C.; Lowenich, D.; Haber, T.; Linder, R.; Kleinermanns, K.; Tatchen, J.; Marian, C. M. *Phys. Chem. Chem. Phys.* **2005,** *7* (16), 3021-3026.

80. Sobolewski, A. L.; Domcke, W.; Hattig, C. *PNAS* **2005,** *102* (50), 17903-17906.

81. Sobolewski, A. L.; Domcke, W. *ChemPhysChem* **2006,** *7* (3), 561-564.

82. Chass, G. A.; Mirasol, R. S.; Setiadi, D. H.; Tang, T. H.; Chin, W.; Mons, M.; Dimicoli, I.; Dognon, J. P.; Viskolcz, B.; Lovas, S.; Penke, B.; Csizmadia, I. G. *J. Phys. Chem. A* **2005,** *109* (24), 5289-5302.

Table 1. Relative energies (C), enthalpies (ΔH_0) and Gibbs energies (ΔG) (in kcal/mol) calculated at different levels of theory for the most stable conformers of GFA tripeptide. Structures are ordered according to ΔG. Labelling according to Figure 1. The relative population (Pop) of conformers according to a Maxwell-Boltzman distribution at T = 300K is also included. Scaled frequencies have been considered for the calculation of the thermodynamical properties.

	CCSD(T)/CBS				ΔE[M06-2X/		RI-DFT-D/TPSS/LP			
Structure	**ΔE[a]**	**ΔH_0[b]**	**ΔG**	**Pop**	**6-311+G(2df,2dp)[c]**	**Structure**	**ΔE**	**ΔH_0[d]**	**ΔG**	**Pop**
GFA_01 [β_L(a)]	2.14	0.00	0.00	1000	0.83	**GFA_04 [β_L(a)]**	4.00	0.00	0.00	1000
GFA_02 [3_{11}]	1.70	0.26	0.06	916	0.95	**GFA_05 [β_L(a)]**	4.08	0.08	0.35	554
GFA_03 [β_L(a)]	2.02	0.01	0.07	894	0.95	**GFA_03 [β_L(a)]**	3.53	0.04	0.52	419
GFA_04 [β_L(a)]	1.72	0.18	0.54	409	1.33	**GFA_02 [3_{11}]**	2.90	0.16	0.53	414
GFA_05 [β_L(a)]	1.80	0.18	0.69	317	1.28	**GFA_01 [β_L(a)]**	3.65	0.07	0.68	319
GFA_06 [$\gamma_L(g^-)$]	0.93	0.28	1.25	125	0.58	**GFA_06 [$\gamma_L(g^-)$]**	1.81	0.02	1.58	70
GFA_07 [$\gamma_L(g^-)$]	0.41	0.3	1.27	122	1.26	**GFA_09 [β_L(a)]**	1.31	0.16	1.74	54
GFA_08 [$\gamma_L(g^+)$]	0.97	0.35	1.47	88	0.68	**GFA_10 [β_L(a)]**	1.19	0.14	1.75	53
GFA_09 [β_L(a)]	0.52	0.2	1.61	69	2.00	**GFA_07 [$\gamma_L(g^-)$]**	1.17	0.09	1.79	50
GFA_10 [β_L(a)]	0.43	0.21	1.65	64	2.09	**GFA_08 [$\gamma_L(g^+)$]**	1.89	0.10	1.96	37
GFA_11 [$\gamma_L(g^+)$]	0.89	0.34	1.73	56	0.70	**GFA_13 [$\gamma_D(g^-)3_{11}$]**	3.12	0.49	2.00	35
GFA_12 [$\gamma_D(g^-)$]	0.54	0.46	1.83	48	0.76	**GFA_14 [γ_L(a)3_{11}]**	3.88	0.30	2.01	35
GFA_13 [$\gamma_D(g^-)3_{11}$]	1.15	0.62	2.34	21	0.92	**GFA_12 [$\gamma_D(g^-)$]**	0.70	0.32	2.24	23
GFA_14 [γ_L(a)3_{11}]	1.00	0.5	2.54	15	1.37	**GFA_11 [$\gamma_L(g^+)$]**	1.79	0.12	2.35	19
GFA_15 [$\gamma_L(g^-)$]	0.00	0.46	2.57	14	1.54	**GFA_16 [$\gamma_D(g^-)$]**	0.71	0.49	3.39	3
GFA_16 [$\gamma_D(g^-)$]	1.46	0.53	2.87	9	0.00	**GFA_15 [$\gamma_L(g^-)$]**	0.00	0.68	3.67	2

[a]Total relative energy evaluated as a sum of CBS RI-MP2 relative energy and the difference between CCSD(T) and MP2 relative energies. [b]ZPVE were calculated at RIMP2/cc-pVDZ level of theory. [c]Single-point energy calculations on RI-MP2/cc-pVTZ geometries. [d]ZPVE were calculated at RI-DFT-D/TPSS/LP level of theory.

Chart 1.

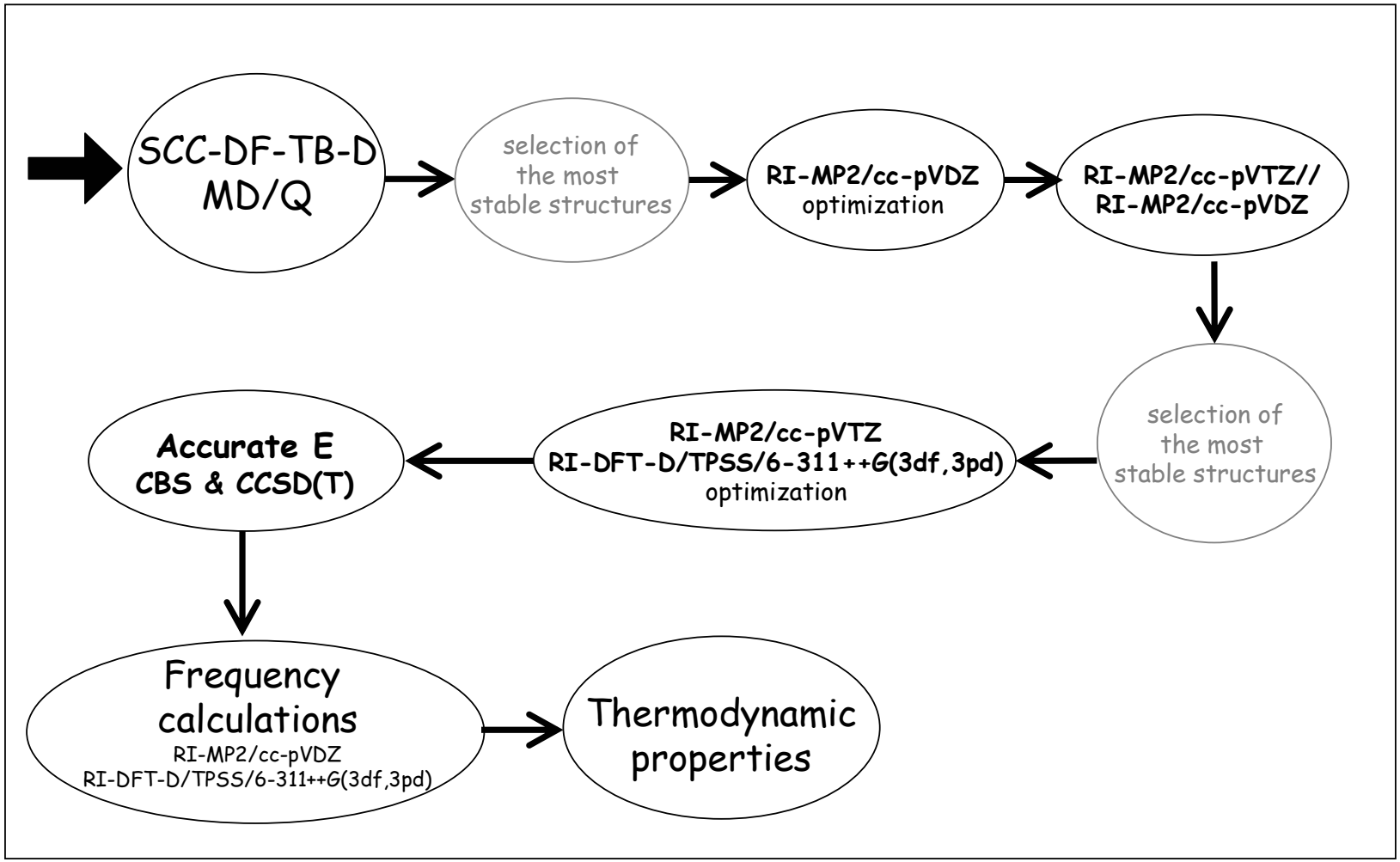
SCC-DF-TB-D
MD/Q
selection of
the most
stable structures
RI-MP2/cc-pVDZ
optimization
RI-MP2/cc-pVTZ//
RI-MP2/cc-pVDZ
selection of
the most
stable structures
RI-MP2/cc-pVTZ
RI-DFT-D/TPSS/6-311++G(3df,3pd)
optimization
Accurate E
CBS & CCSD(T)
Frequency
calculations
RI-MP2/cc-pVDZ
RI-DFT-D/TPSS/6-311++G(3df,3pd)
Thermodynamic
properties

Chart 2.

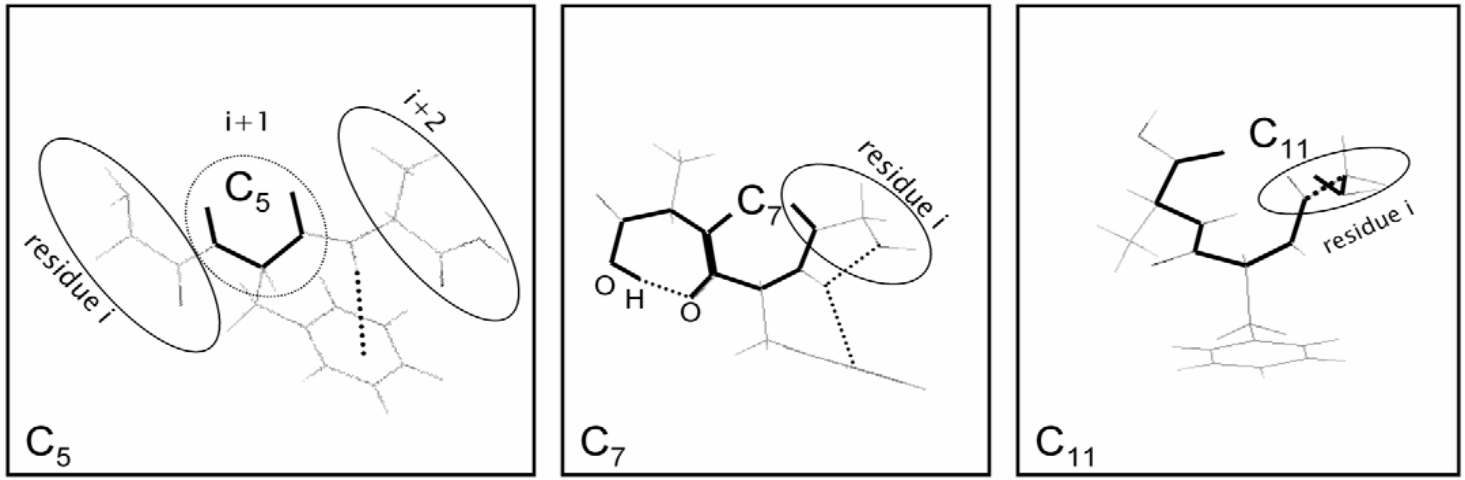

Chart 3.

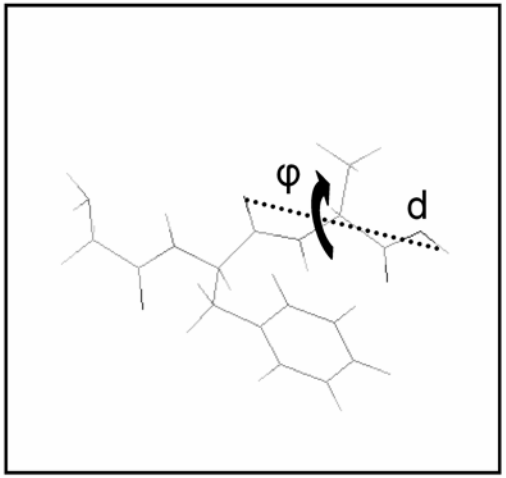

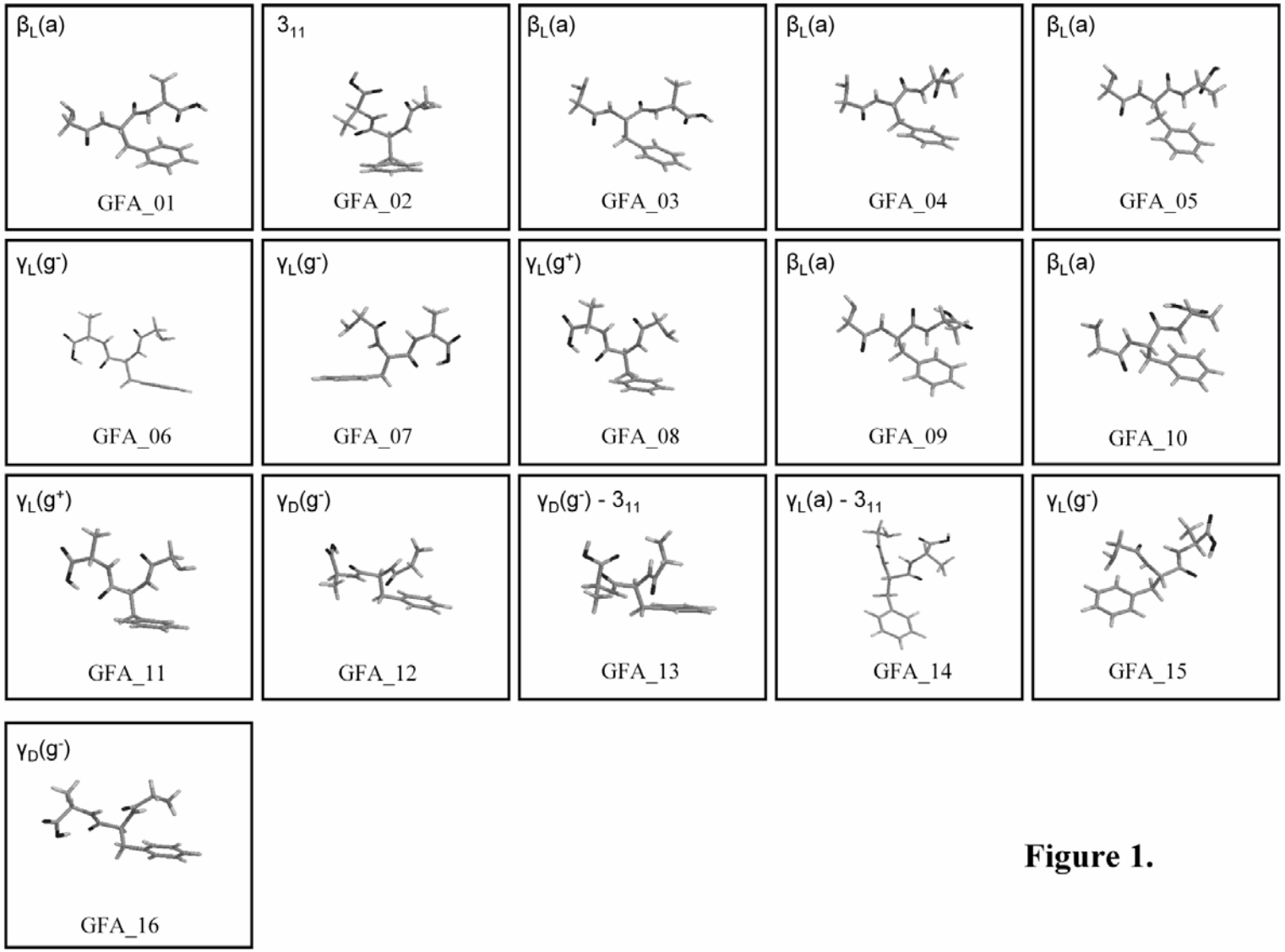
βL(a)
GFA_01
3₁₁
GFA_02
βL(a)
GFA_03
βL(a)
GFA_04
βL(a)
GFA_05
γL(g⁻)
GFA_06
γL(g⁻)
GFA_07
γL(g⁺)
GFA_08
βL(a)
GFA_09
βL(a)
GFA_10
γL(g⁺)
GFA_11
γD(g⁻)
GFA_12
γD(g⁻) - 3₁₁
GFA_13
γL(a) - 3₁₁
GFA_14
γL(g⁻)
GFA_15
γD(g⁻)
GFA_16

Figure 1.

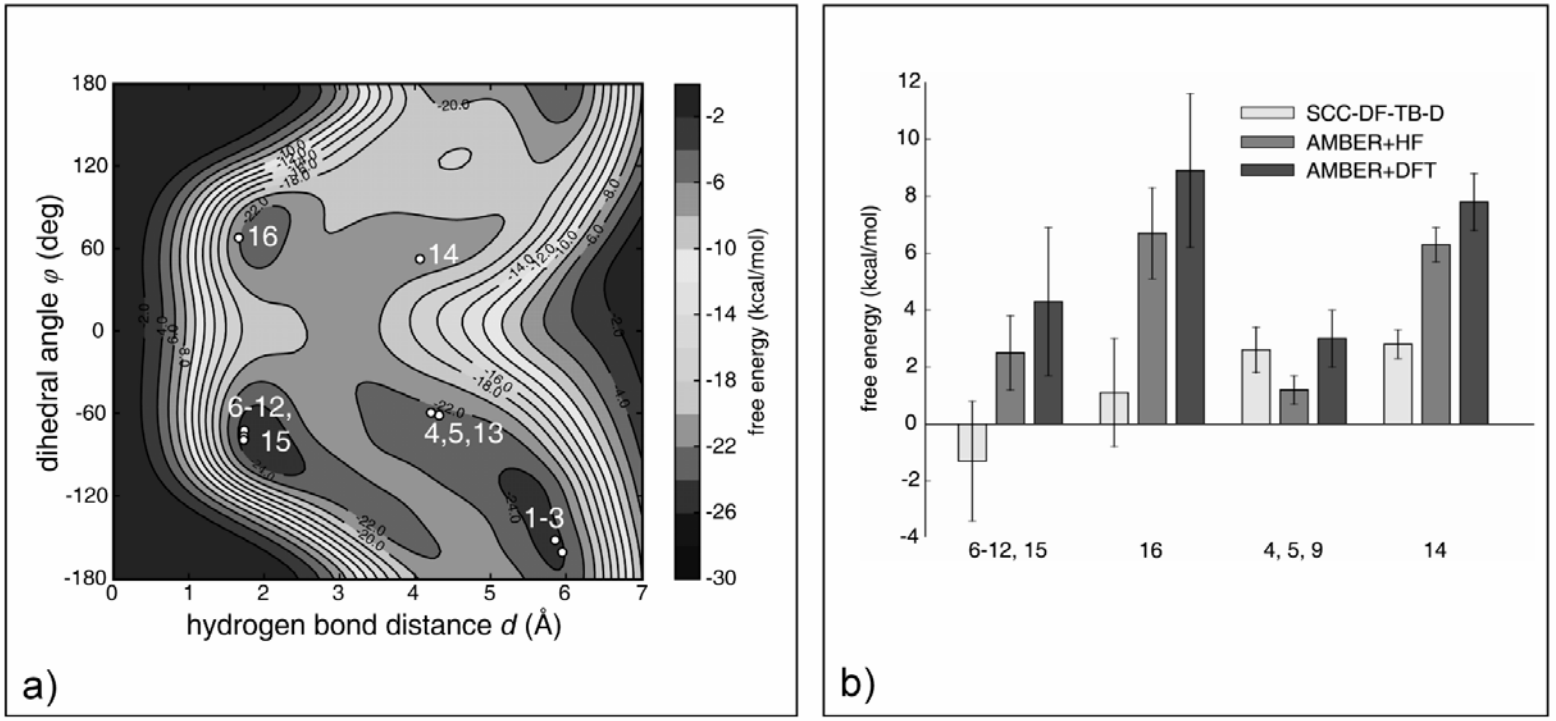
a)
dihedral angle φ (deg)
hydrogen bond distance d (Å)
free energy (kcal/mol)
16
14
6-12,
15
4,5,13
1-3
b)
free energy (kcal/mol)
SCC-DF-TB-D
AMBER+HF
AMBER+DFT
6-12, 15
16
4, 5, 9
14

Figure 2.

Figure 3.

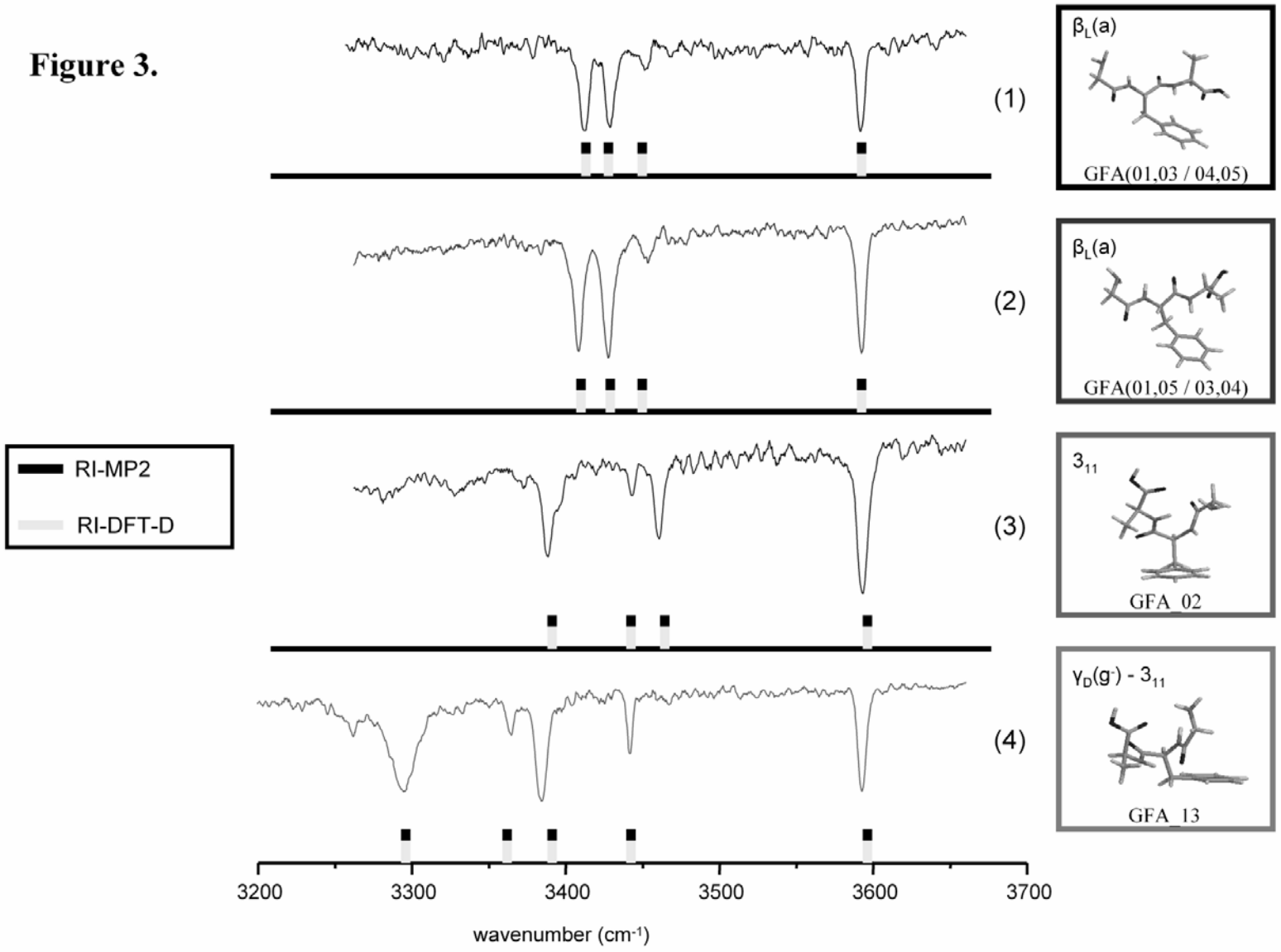
RI-MP2
RI-DFT-D
(1)
(2)
(3)
(4)
β_L(a)
GFA(01,03 / 04,05)
β_L(a)
GFA(01,05 / 03,04)
3_{11}
GFA_02
$\gamma_D(g^-)$ - 3_{11}
GFA_13
3200
3300
3400
3500
3600
3700
wavenumber (cm^{-1})

Figure 4.

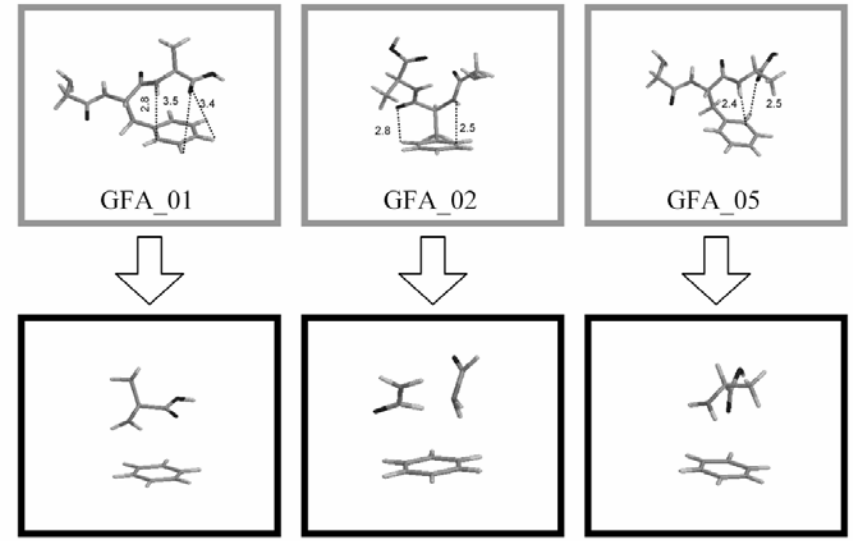
2.8
3.5
2.4
GFA_01
2.8
2.5
GFA_02
2.4
2.5
GFA_05

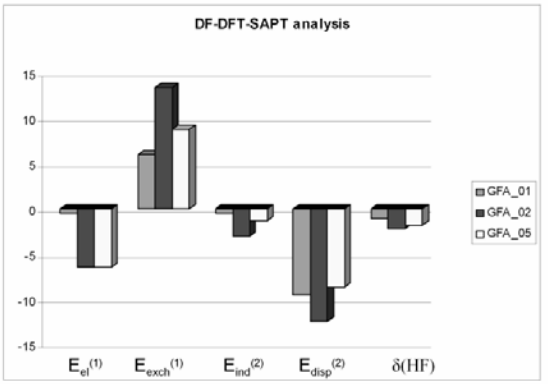
DF-DFT-SAPT analysis
15
10
5
0
-5
-10
-15
GFA_01
GFA_02
GFA_05
$E_{el}^{(1)}$
$E_{exch}^{(1)}$
$E_{ind}^{(2)}$
$E_{disp}^{(2)}$
δ(HF)

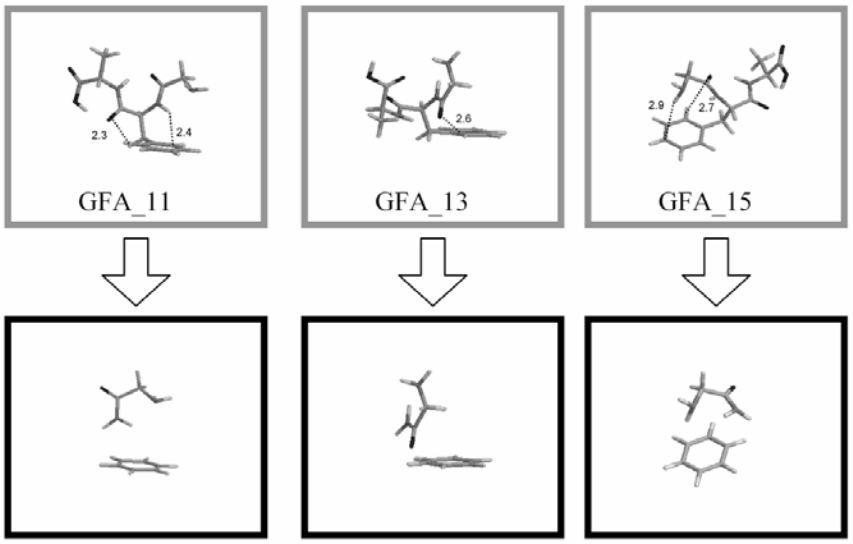
2.3
2.4
GFA_11
2.6
GFA_13
2.9
2.7
GFA_15

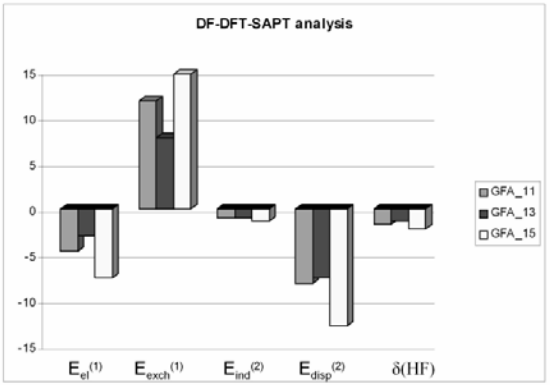
DF-DFT-SAPT analysis
15
10
5
0
-5
-10
-15
GFA_11
GFA_13
GFA_15
$E_{el}^{(1)}$
$E_{exch}^{(1)}$
$E_{ind}^{(2)}$
$E_{disp}^{(2)}$
δ(HF)

TOC

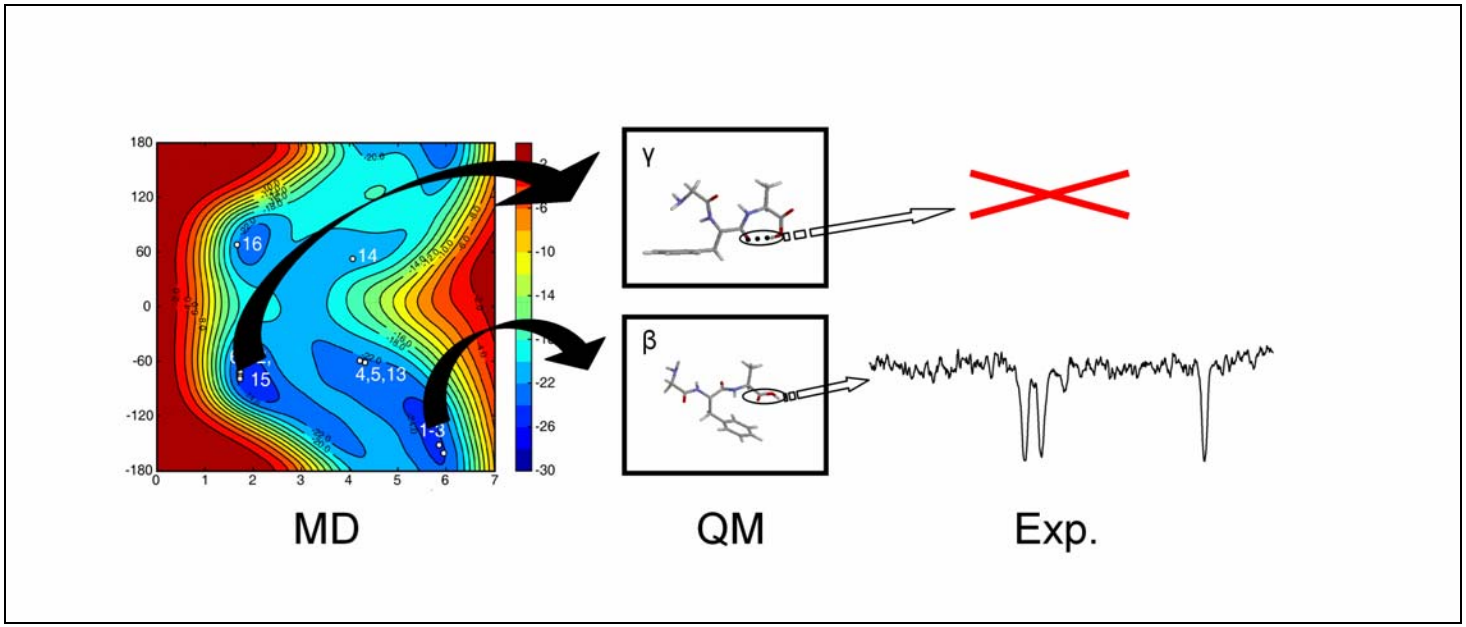
180
120
60
0
-60
-120
-180
0 1 2 3 4 5 6 7
16
14
15
4,5,13
1-3
-6
-10
-14
-22
-26
-30
γ
β
MD
QM
Exp.